INVITED ARTICLE

EPR study of the polydomain structure of the twist-bend nematic phase of CB9CB in the bulk

Corrado Bacchiocchi[a*], Maria-Gabriela Tamba[b], Georg H. Mehl[b], Alberto Arcioni[c], Isabella Miglioli[c] and Claudio Zannoni[c]

[a]School of Science and Technology, Chemistry Division, University of Camerino, Via S. Agostino 1, I-62032 Camerino (MC), Italy; [b]Department of Chemistry, University of Hull, Hull HU6 7RX, UK; [c]Dipartimento di Chimica Industriale "Toso Montanari", Università di Bologna, Viale Risorgimento 4, I-40136 Bologna, Italy

ABSTRACT
EPR spin probe spectra of the liquid crystal phases exhibited, in the bulk, by the $1''$,$9''$-bis(4-cyanobiphenyl-4$'$-yl)nonane (CB9CB) bent-shape dimer showed that, on cooling from the isotropic phase, this material forms a uniaxial nematic phase with a uniform director macroscopically aligned along the spectrometer field. Upon further cooling, a transition into the twist-bend nematic phase is observed, after a biphasic region of about 4 K. In this lower temperature nematic phase, the director does not appear to be macroscopically aligned. The non uniform director distribution is modelled as a collection of monodomains, tilted with respect to the magnetic field and orientationally distributed around the tilt direction.

1. Introduction

The recent systematic synthesis and phase characterization of several bent-shape bimesogens [1–7] has brought the total number of materials known to exhibit the twist-bend nematic phase, N_{tb}, to well over one hundred [1]. The N_{tb} phase has been found most often in bent-shape bimesogens composed by rigid mesogenic moieties joined by a flexible linker and only in a few rigid bent-core liquid crystals (LCs) [8,9]. This body of work confirms the previous suggestion [8,10–13] that the main feature responsible of the stabilization of the N_{tb} phase is the overall molecular curvature.

The observed strong dependence of the stability of the N_{tb} phase on the bend angle was predicted by generalised Maier-Saupe theories proposed by Greco et al. [14] for rigid bent-core bimesogens and by Vanakaras et al. [15] for bimesogens with intramolecular torsion. More recently, Ferrarini extended [16] the previous model [14] to include a distribution of bend angles. The study showed that a broader distribution is expected to decrease the stability of the N_{tb} phase, as supported by recent experimental evidence [7,17,18], and pointed out that effects of electrostatic nature are not an essential ingredient to explain the existence of the N_{tb} phase. A generalisation of the

CONTACT Corrado Bacchiocchi. Email: corrado.bacchiocchi@unicam.it

work of Greco et al. [14], carried out by Tomczyk et al. [19], showed that the biaxiality of the two mesogenic moieties can affect the N_{tb} phase stability, but the bend angle is still the determinant factor.

If the incidence of the N_{tb} phase formed by bent-shape bimesogens needs to be further clarified, the debate over the general structure of the phase has been settled by a recent article from Zhu et al. [20]. This was the first "direct" measurement of nanometric helical pitch, previously revealed by freeze-fracture transmission electron microscopy measurements [21,22] and electroclinic effect measurements [23], and provided a more direct identification of the heliconical nematic structure, initially proposed by Cestari et al. [24], where the phase is macroscopically uniaxial with a local nematic director that makes a constant tilt angle θ_0 with respect to a macroscopic axis and twists around it in an helical fashion. In their work Zhu et al. [20] have used resonant soft X-ray scattering at the carbon K-edge to study the N_{tb} phase of CB7CB in the bulk and found a spatial periodicity of around 8–10 nm of the molecular orientation without electron density modulation. Interestingly, the sample was not macroscopically aligned but appeared to be a collection of well ordered uniaxial domains of variable size and different orientation of the heliconical axis.

Very recently, a work by Stevenson et al. [25] used resonant "hard" X-ray scattering at the selenium K-edge to investigate the N_{tb} phase of the difluoroterphenyl dimer DTC5C7 in the bulk. The study found a spatial periodicity of around 9–12 nm of the molecular orientation without electron density modulation, further confirming the previous evidence in favour of the heliconical nematic structure. Moreover, the heliconical axis of the N_{tb} phase was macroscopically aligned by a magnetic field of 1 T resulting in a $\langle P_2 \rangle$ of the axis that was estimated to be very close to unity. Thanks to this alignment the Authors were able to obtain a molecular-level model of the N_{tb} phase, including a determination of the tilt angle of the mesogens relative to the helix axis.

We have recently proposed a model of an orientational distribution capable of describing the nonuniform alignment of the tilted local director with respect to the magnetic field observed in EPR spectra of the N_{tb} phase of the dimer $1''$,$11''$-bis(4-cyanobiphenyl-4'-yl)undecane (CB11CB) [26]. From the analysis of the spectra of a suitable stable nitroxide free radical dissolved in the LC host, it was possible to recover molecular-level information about the local order in the mesophases, their reorientational dynamics, the tilt angle and the orientational distribution of the heliconical domains in the N_{tb} phase.

In this article the EPR spin probe technique [27–29] is employed to study the mesophases exhibited by the odd symmetric LC dimer $1''$,$9''$-bis(4-cyanobiphenyl-4'-yl)nonane (CB9CB) to show that the above molecular-level information can be consistently recovered also for this homologue and to help establish the EPR technique as a tool that can provide very useful structural and dynamic information in a relatively straightforward and efficient way that appears to be well-suited for a systematic study of the increasing number of liquid crystal dimers, oligomers and possibly polymers exhibiting the N_{tb} phase.

The structure of the article is as follows. The next section reports the experimental details. The Theory section briefly describes the models used to analyse the EPR spectra. In the Results and Discussion section the information recovered from the analyses are exposed and finally, in the Conclusions section, a summary of the main findings is presented.

2. Experimental

The LC dimer CB9CB is formed by two cyanobiphenyl groups linked by an alkyl chain of nine carbon atoms, as first reported in [30]. It was synthesized in the Department of Chemistry at the University of Hull (UK) and was used without further purification. Its molecular structure is shown in Figure 1.
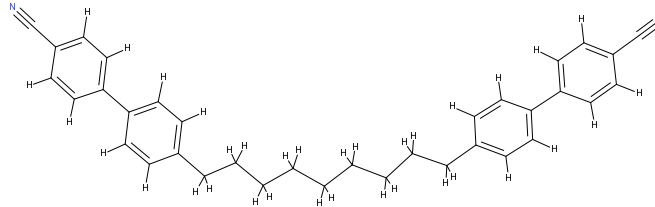
Figure 1. Molecular structure of CB9CB.

Upon cooling from the isotropic (I) phase, the CB9CB LC exhibits a transition to the ordinary, uniaxial nematic phase (N_u) and, on further cooling, to the N_{tb} phase.

The phase sequence of this material was studied by Tripathi et al. [31] via high-resolution adiabatic scanning calorimetry at the low scanning rate of 0.15 K/h and it was N_{tb} – 377.22 K – N_u – 392.92 K – I. More recently, Robles-Hernández et al. [32], using modulated DSC at 1 K/min, found the following transition temperatures: Crystal – 357.6 K – N_{tb} – 379.09 K – N_u – 394.92 K – I, where the N_{tb}–N_u and the N_u–I transitions were about 2 K higher.

The nitroxide spin probe, used for doping the CB9CB LC, was the 3β-doxyl-5α-cholestane free radical (Aldrich, hereafter referred to as CSL). This was employed in a number of previous studies [26,28,33–35] where it proved to be a reliable probe to monitor the order and the dynamics of the LC system, due to its size, morphology and rigidity, which results in a strong orientation by the LC host. The CSL structure is shown in Figure 2 together with the chosen ordering (x,y,z, solid line) and magnetic (x',y',z', dashed line) molecular frames and the indication of its two main reorientational motions, tumbling and spinning, with the corresponding components of the rotational diffusion tensor: $D_\perp$ (reorientation of the molecular long axis) and $D_\parallel$ (rotation around the long axis), respectively.
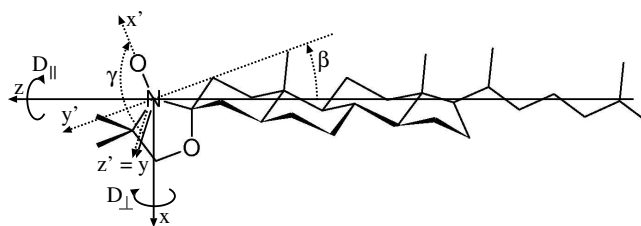
Figure 2. Molecular structure of the CSL spin probe together with the chosen ordering $(x, y, z$, solid line) and magnetic $(x', y', z'$, dashed line) molecular frames, the Euler angles, β and γ, between the molecular frames and the principal components, $D_\perp$ (reorientation of the molecular long axis) and $D_\parallel$ (rotation around the molecular long axis), of the rotational diffusion tensor.

CSL was added to CB9CB in the I phase at a typical concentration of about 1×10^{-4} g_{CSL}/g_{CB9CB}, which is below the limiting concentration typically suggested [27] to avoid Heisenberg spin exchange distortion effects.

Samples of CSL-doped CB9CB were inserted into glass capillaries of 1.8 mm internal

diameter for the EPR measurements. EPR spectra were acquired with a Bruker EMX spectrometer equipped with an ER 041XG microwave X-band (9.5 GHz) Gunn Diode bridge and a rectangular ER 4102ST cavity. The samples were thermostated with a nitrogen flux through a variable temperature unit Bruker B-VT 2000. The temperature was monitored with a calibrated type T thermocouple (Comark Ltd.) kept in close proximity with the sample and showed a stability better than ± 0.05 K.

The molecular magnetic frame (x', y', z') was chosen according to the standard system of coordinates for the N–O paramagnetic moiety with the x' axis along the N–O bond [35,36] and the z' axis perpendicular to the five-membered ring, i.e. parallel to the p_z orbital containing the unpaired electron. According to a standard approach, the z axis of the molecular ordering frame is considered parallel to the principal axis of inertia of the probe (its "long axis") and, to simplify the rotation which takes the ordering into the magnetic frame [35,36], the y axis is considered parallel to the z' axis. To reduce the correlation among variable parameters, the Euler angles, β and γ, between the molecular frames, were fixed in the fittings to 15° and 90°, respectively, in agreement with previous results obtained in related systems [28,33–36].

3. Theory

The explicit form of a simple probability density distribution, $P(\alpha, \beta_{\mathrm{d}})$, capable of describing the nonuniform alignment of the tilted local domain director with respect to the magnetic field observed in EPR spectra of a bent-shape bimesogen in the N_{tb} phase has been obtained in a previous work [26]

$$P(\alpha, \beta_{\mathrm{d}}) = \exp\left[\lambda_{\mathrm{d}}\left(\frac{3}{2}f(\alpha, \beta_{\mathrm{d}}) - \frac{1}{2}\right)\right], \tag{1}$$

where λ_{d} is a positive constant and

$$f(\alpha, \beta_{\mathrm{d}}) = \frac{\sec^2\theta_0\left(\cos\beta_{\mathrm{d}} - \cos\alpha\tan\theta_0\sqrt{\cos^2\alpha\sin^2\theta_0 - \cos^2\beta_{\mathrm{d}} + \cos^2\theta_0}\right)^2}{\left(1 + \cos^2\alpha\tan^2\theta_0\right)^2}. \tag{2}$$

Here, β_{d} is the angle between the local domain director and the magnetic field, θ_0 is the tilt angle and α is the azimuthal angle around the tilt direction whose distribution, for simplicity, has been assumed to be uniform.

The EPR spectrum of the CSL spin probe in the N_{tb} phase, $I_{N_{\mathrm{tb}}}(\omega - \omega_0)$, is modelled as a superposition of uniaxial nematic domain spectra, $I(\omega - \omega_0, \beta_{\mathrm{d}})$

$$I_{N_{\mathrm{tb}}}(\omega - \omega_0) = \int_\alpha \int_{\beta_{\mathrm{d}}} I(\omega - \omega_0, \beta_{\mathrm{d}}) P(\alpha, \beta_{\mathrm{d}}) \, \mathrm{d}\alpha \, \mathrm{d}\beta_{\mathrm{d}}, \tag{3}$$

where $I(\omega - \omega_0, \beta_{\mathrm{d}})$ is the unsaturated, high-field EPR spectrum at frequency ω, which is calculated using the classic Stochastic Liouville Equation approach of Freed and collaborators [27,37,38] which predicts that

$$I(\omega - \omega_0, \beta_{\mathrm{d}}) = \frac{1}{\pi}\left\langle\left\langle v \left| \left[\left(\hat{\mathbf{\Gamma}} - i\mathcal{L}\right) + i(\omega - \omega_0)\mathbf{I}\right]^{-1} \right| v\right\rangle\right\rangle, \tag{4}$$

4

in the assumption that the CSL spin probe reorients in a locally uniaxial nematic domain whose director, $\boldsymbol{n}$, forms with the spectrometer uniform magnetic field an angle β_d. The central frequency, ω_0, at the spectrometer field, B_0 (0.339 T), is obtained from the g factor, g_0, and the Bohr magneton, β_e: $\omega_0 = g_0\beta_e B_0/\hbar$. $\mathcal{L}$ is the Liouville superoperator obtained from the orientation dependent spin Hamiltonian, $\hat{\boldsymbol{\Gamma}}$ is the diffusion superoperator describing the reorientational motion of the probe, $|v\rangle$ is a vector containing spin transition moments averaged over the equilibrium ensemble and $\boldsymbol{I}$ is the identity. A brief account of the general approach of Freed and collaborators [27,37,38] has been presented in a previous work [28]. To reduce the total number of model parameters, the reorientational motion of the probe is assumed to take place in a uniaxial, mean field ordering potential

$$U(\beta) = -kT\left[\lambda_{20}P_2(\cos\beta)\right] \ , \tag{5}$$

where λ_{20} is the strength of the potential, k the Boltzmann constant, T the temperature in Kelvin and $P_2(\cos\beta)$ is a second rank Legendre polynomial. The local order is described by the orientational order parameter, $\langle P_2\rangle$, defined as

$$\langle P_2\rangle = \frac{\int P_2(\beta)\,\exp[-U(\beta)/kT]\,\sin\beta\,\mathrm{d}\beta}{\int \exp[-U(\beta)/kT]\,\sin\beta\,\mathrm{d}\beta} \ , \tag{6}$$

where β is the probe orientation with respect to the local domain director.

The order of the local director with respect to the tilt direction is described by the orientational order parameter, $\langle P_2\rangle_d$, which has been defined in the previous work [26]. A value of $\langle P_2\rangle_d = 0$ represents the limiting case of an isotropic distribution of the domain directors, whereas in the other limit of $\langle P_2\rangle_d = 1$, the local director is uniformly oriented along the tilt direction, i.e. at a fixed angle θ_0.

The integration of equation 3 along both α and β_d was carried out numerically using the adaptive multidimensional integration Fortran routine DCUHRE [39]. The EPR spectra simulation program employed was based on a set of Fortran routines implementing the slow tumbling theory for a spin probe reorienting in a LC, developed by Freed and collaborators [27,37,38], combined with a software package [40] that optimizes the fit parameters using the Gauss-Newton-Marquardt non-linear least squares method [41].

4. Results and Discussion

In previous studies we have shown that CSL is a reliable probe that can quite accurately monitor the local molecular order, the reorientational dynamics and the local director distribution of various LCs and, in particular, of the 5CB LC [42,43]. A good agreement between the order parameter of the probe and of the LC host was also reported by Oganesyan et al. via molecular dynamics simulations of the CSL probe in 5CB [44]. Unfortunately, despite the chemical similarity of the CB9CB dimer to 5CB it is not possible to assume that CSL will be also able to correctly report the molecular organization of CB9CB. This ability depends essentially on the local chemical environment experienced by the probe in the LC host. Information about the chemical environment in which an EPR spin probe is located can be obtained from a rigid-limit spectrum. Such a spectrum is typically recorded at a temperature at which the sample is solid and molecular reorientations are frozen on the experimental time

scale. In these conditions the spectral lineshapes and the positions of the peaks are determined only by the hyperfine tensor which, in turn, depends on the polarity of the environment. A rigid-limit spectrum of CB9CB was recorded in the bulk at 173.2 K and is reported in Figure 3 together with the rigid-limit bulk spectrum of 5CB at the same temperature. The positions of the peaks in the CB9CB spectrum are identical to the corresponding positions in the 5CB spectrum and the spectral lineshapes are very similar. This result indicates that the chemical environment experienced by CSL in the CB9CB dimer is very similar to that in 5CB, therefore it is reasonable to expect that CSL will be also a reliable probe of the molecular organization of the dimer.
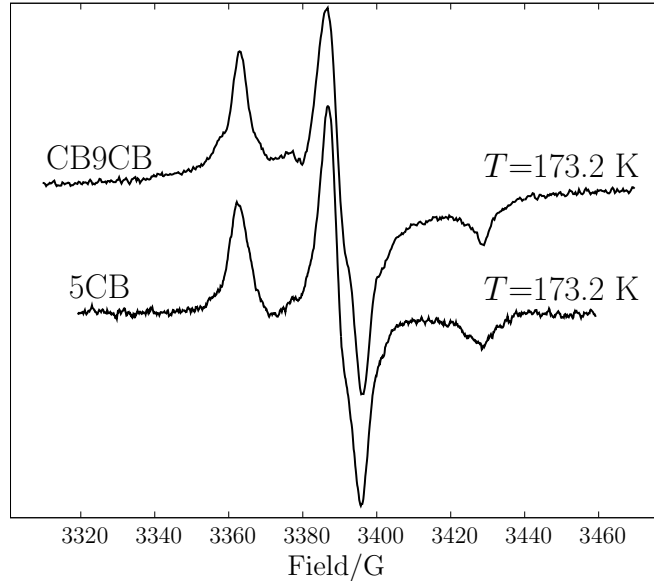
Figure 3. Rigid-limit spectrum of CB9CB compared with a rigid-limit spectrum of 5CB. Both spectra were recorded in the bulk at 173.2 K.

The phase behaviour exhibited by the CB9CB LC was studied by recording a series of EPR spectra, on cooling, starting at a temperature of 413.2 K and cooling to 343.2 K. In this temperature interval, the observed phase behaviour, that will be discussed in detail below, was as follows: N_{tb} – 373.2 K – N_u – 389.2 K – I, with a downshift of the transition temperatures of about 4 K with respect to the values determined by Tripathi et al. [31]. Previous studies of the related LC CB7CB in presence of a small amount of a dopant [45,46] also found downshifts of the transition temperatures of a few K. The N_u–I transition temperature was determined as the mean between the lowest temperature in the I phase (390.2 K) and the highest temperature in the N_u phase (388.2 K). The N_{tb} phase was found to coexist with the N_u phase in the range 375.2–371.2 K. The centre of this interval was taken as the N_{tb}–N_u transition temperature, $T_{N_{tb}-N_u}$.

The isotropic model was employed to fit in a consistent way the EPR spectra recorded in the temperature interval 413.2–390.2 K (see Figure 4, black line: experimental, red line: fit). These are clearly fast motional spectra exhibiting three well-resolved hyperfine lines typical of an isotropic phase. The distance between the central and the outer peaks is quite constant across the phase and corresponds to 14.7 G (1 T = 10^4 G) at 413.2 K which is very similar to the value of 14.6 G that we have found in the fast motional regime of the isotropic phase of 5CB in the bulk.

The distance between the central and the outer peaks showed a marked decrease

at the temperature of 388.2 K, suggesting the occurrence of a phase transition. In the temperature interval 388.2–377.2 K the lineshapes exhibited small and consistent changes expected for a uniaxial nematic phase forming a monodomain uniformly aligned along the magnetic field. As expected, spectra in this temperature interval could be consistently fitted to the uniaxial nematic monodomain model. EPR spectra of this uniaxial nematic phase are shown in Figure 5 (black line: experimental, red line: fit).

At temperatures lower than 377.2 K it was no longer possible to obtain a consistent fit to the uniaxial nematic monodomain model. By a careful inspection of the spectra, the uniaxial nematic spectral contribution appeared to decrease while a new contribution was appearing, suggesting the onset of a new phase coexisting with the N_u phase. A small biphasic region, across the N_{tb}–N_u phase transition, has been previously observed by Tripathi et al. [31] for pure CB9CB and its mixtures with 5CB and is consistent with the observed weakly first order nature of the N_{tb}–N_u transition. Previous works on the related LC CB7CB [45,46] also showed the presence of a biphasic region, induced by a small amount of a dopant.

Following these findings, spectra recorded at 377.2 K or below were fitted to a model formed by two spectral contributions. One contribution, due to the N_u phase, was calculated according to the same uniaxial nematic monodomain model employed in the interval 388.2–377.2 K; the other contribution, due to the N_{tb} phase, was calculated according to the distributed tilt (DT) model presented earlier [26].

The extent of the temperature interval of the biphasic region was initially roughly estimated by observing that in spectra recorded below 371.2 K the signature lineshapes of the uniaxial nematic spectral contribution were no longer present and that spectra recorded below 371.2 down to 366.2 K appeared to be fairly similar, suggesting that the system was not experiencing further phase changes.

Spectra recorded in the temperature interval 377.2–366.2 K were then included in a global analysis, to reduce the correlation among the increased number of fit parameters. This was performed by adopting a globalization scheme based on the assumption that the order parameters are constant with temperature when the N_u and the N_{tb} phases are in equilibrium. Accordingly, the local order parameter, $\langle P_2 \rangle$, of the N_u and the N_{tb} phases, the order parameter of the domain directors, $\langle P_2 \rangle_d$, and the tilt angle, θ_0, of the N_{tb} phase were considered as global parameters. Moreover, in a preliminary analysis, the local order of the N_u and the N_{tb} phases in equilibrium was assumed to be the same, therefore the local $\langle P_2 \rangle$ was fitted to a single variable parameter. Given the increased complexity of a model formed by two spectral contributions, the choice of the initial values of the fit parameters (guess) was determinant to ensure a reliable and meaningful analysis. Guess value for the local $\langle P_2 \rangle$ of the N_u and the N_{tb} phases was 0.44 which corresponded to the best-fit value of $\langle P_2 \rangle$ of the spectrum recorded at 377.2 K, analysed with the uniaxial nematic monodomain model. Guess value for the order parameter of the domain directors, $\langle P_2 \rangle_d$, was 0.5 which corresponded to typical values of $\langle P_2 \rangle_d$ found in the analyses of spectra of the N_{tb} phase of the related LC CB11CB presented earlier [26]. Guess value for the tilt angle, θ_0, was 1.0° according to the result of Robles-Hernández et al. [32], where θ_0 was zero at the onset of the N_{tb} phase. Guess value for the molecular-level reorientational dynamics, represented by the perpendicular component of the rotational diffusion tensor, $D_\perp$, was 0.027 ns^{-1} which corresponded to the best-fit value of $D_\perp$ of the spectrum recorded at 377.2 K, analysed with the uniaxial nematic monodomain model. This value was used as guess for both the N_u and the N_{tb} phases across the temperature interval 377.2–366.2 K. Guess values for the fractional contribution of the spectral component due

to the N_{tb} phase, f_{tb}, were obtained from a series of preliminary global analysis, carried on without optimization, of the spectra recorded between 377.2 and 366.2 K. In these analyses, all other parameters were kept fixed while the f_{tb} values, at the various temperatures, were systematically varied manually until a satisfactory visual fit was obtained. A further preliminary global analysis of the spectra recorded in the temperature interval 377.2–366.2 K, this time with optimization, was then performed. Best-fit parameters showed a consistent temperature behaviour with an overall good quality of the fits (not shown). This analysis narrowed the range of the biphasic region by showing that f_{tb} was essentially zero at 377.2 K, as expected, and was very close to unity at 368.2 K and below. Best-fit parameters of this global analysis were then used as guesses for a further global analysis, with optimization, of spectra between 377.2 and 368.2 K. In this analysis, the local order parameters $\langle P_2 \rangle$ of the N_u and the N_{tb} phases were optimized independently. Best-fit parameters showed only small differences from those recovered from the previous analysis. In particular, f_{tb} was very close to zero at 377.2 K and very close to unity at 368.2 K, further narrowing the biphasic region in the interval between 375.2 and 371.2 K. The $\langle P_2 \rangle$ of the N_u phase was 0.43 and was similar, as expected, to the value of 0.39 obtained for the N_{tb} phase. The $\langle P_2 \rangle_d$ was 0.55 and the tilt angle, θ_0, was 0.1° i.e. close to zero, as expected. The molecular-level reorientational dynamics, represented by the perpendicular component of the rotational diffusion tensor, $D_\perp$, of the N_{tb} phase (shown below) was slower than that of the N_u phase. This result is in agreement with our previous observation on the molecular-level reorientational dynamics of the related LC CB11CB [26] but, arguably, is not sufficient, by itself, to explain the very large decrease of the field-induced director dynamics observed in the N_{tb} phase of the CB11CB LC [47] and in the homologues CB9CB [48] and CB7CB [49]. This interesting point is further discussed below, when the temperature dependence of $D_\perp$ across the N_u and N_{tb} phases is presented.

The previous global analysis was then repeated using as guesses for the tilt angle, θ_0, values ranging from 0.5° to 10°. All analyses gave very similar best-fit parameters, within 1% of the values presented above, assessing the robustness of the fit. EPR spectra in the biphasic region are shown in Figure 6 (black line: experimental, red line: fit). The temperature dependence of the fractional contribution of the spectral component due to the N_{tb} phase, f_{tb}, across the biphasic region of CB9CB, obtained from the above global fit, is presented in Figure 7.

Spectra in the N_{tb} phase, below the biphasic region, in the temperature interval 368.2–343.2 K, were analysed with the distributed tilt (DT) model presented earlier [26]. A series of preliminary analyses showed a relatively large correlation between the local order parameter, $\langle P_2 \rangle$, and the tilt angle, θ_0. To limit this correlation, all the spectra in this temperature interval were included in a global analysis by assuming $\langle P_2 \rangle$ independent of the temperature and treated as a global parameter. This assumption appears to be reasonable according to previous studies [32,48,50] where the CB9CB $\langle P_2 \rangle$ exhibited a relatively small variation across the N_{tb} phase. Guess values for the $\langle P_2 \rangle$ and the $\langle P_2 \rangle_d$ were 0.39 and 0.55, respectively, obtained from the global fit in the biphasic region for the N_{tb} phase. Guess values for the tilt angle, θ_0, were taken from the Haller-type θ_0 temperature dependence obtained by Robles-Hernández et al. [32], with the zero of the Haller function shifted at 368.2 K, which corresponds to the first temperature recorded in the N_{tb} phase, below the biphasic region. Guess value for the perpendicular component of the rotational diffusion tensor, $D_\perp$, was taken as the best-fit value at the lowest temperature of the biphasic region.

With this globalization scheme, the overall quality of the fits was good and the recovered best-fit parameters showed a small correlation and a consistent and mean-

ingful temperature dependence, with a best-fit $\langle P_2 \rangle$ of 0.61, in keeping with previous results [32,48,50], and a $\langle P_2 \rangle_d$ of 0.50. Six EPR spectra (black line), between 363.2 and 348.2 K, and the corresponding fits to the DT model (red line) are shown in Figure 8.

The temperature dependence of the local $\langle P_2 \rangle$, across the full temperature range studied, is presented in Figure 9, open squares.

The dependence of the molecular-level reorientational dynamics, represented by the perpendicular component of the rotational diffusion tensor, $D_\perp$, on the reduced temperature, $T^* \equiv T/T_{\mathrm{N_{tb}-N_u}}$, across the $\mathrm{N_{tb}}$ and $\mathrm{N_u}$ phases, is shown in Figure 10 (squares), compared to the values obtained for the related LC CB11CB [26] (circles). In the $\mathrm{N_u}$ phase, values for the CB9CB LC (open squares) were essentially identical to those for the CB11CB LC (open circles). Across the biphasic region, the reorientational dynamics of the $\mathrm{N_{tb}}$ phase (solid symbols) was slower than that of the $\mathrm{N_u}$ phase (open symbols). Finally, in the $\mathrm{N_{tb}}$ phase, the reorientational dynamics of both LCs had values of the same order of magnitude and showed a further, almost linear decrease with the temperature. This significant reduction of the dynamics in the $\mathrm{N_{tb}}$ phase at molecular-level, which is related to an increase of the microscopic rotational viscosity of the phase, is nonetheless quite small when compared to the decrease of several orders of magnitude of the field-induced director dynamics, which corresponds to a very large increase of the macroscopic rotational viscosity, observed in the $\mathrm{N_{tb}}$ phase of the CB11CB LC [47] and in the homologues CB9CB [48] and CB7CB [49]. A very large increase of the macroscopic viscosity accompanied by only a relatively small increase of the microscopic viscosity suggests that, when the system goes from the $\mathrm{N_u}$ to the $\mathrm{N_{tb}}$ phase, the molecular scale environment experiences only a small change whereas, at a larger scale, the system undergoes a much larger transformation. The difference between microscopic and macroscopic viscosity in the $\mathrm{N_{tb}}$ phase has been recently discussed by Cifelli et al. [49]. In this work the Authors measured the molecular translational self-diffusion coefficient in the $\mathrm{N_u}$ and $\mathrm{N_{tb}}$ phases of CB7CB via NMR diffusometry and the macroscopic rotational viscosity of the phases via field-induced director dynamics. The self-diffusion coefficient showed a decrease, with no discontinuity, on going from the $\mathrm{N_u}$ to the $\mathrm{N_{tb}}$ phase, whereas the macroscopic viscosity increased by several orders of magnitude.

The dependence of the tilt angle, θ_0, on the reduced temperature in the $\mathrm{N_{tb}}$ phase, obtained with the globalization scheme described above, is presented in Figure 11 (open squares). Values obtained at the first two temperatures close to the biphasic region showed a relatively larger correlation between the local $\langle P_2 \rangle$ parameter and θ_0 and have been removed. To study the effect of this correlation, the previous global fit was repeated with a second globalization scheme for $\langle P_2 \rangle$ whose temperature dependence was described by the following empirical Haller-type [51] function

$$\langle P_2 \rangle(T) = \langle P_2 \rangle_0 (1 - T/T_{NI})^\beta, \tag{7}$$

where T_{NI}, the temperature of the observed $\mathrm{N_u}$–I transition, was fixed at 389.2 K whereas $\langle P_2 \rangle_0$ and the exponent, β, were obtained by fitting the Haller equation 7 to the $\langle P_2 \rangle$ temperature dependence, in the range 389.2–343.2 K, presented in Figure 9 (open squares). Best-fit parameters were $\langle P_2 \rangle_0 = 0.97$ and $\beta = 0.21$. The corresponding Haller function is shown as a solid line in Figure 9. The overall quality of the fits obtained from this second globalization scheme was similar to the previous one. The recovered temperature dependence of θ_0 was only slightly different from the previous one and is also shown in Figure 11 (solid squares), compared to the values obtained for the related LC CB11CB [26] (open circles) and the Haller-type θ_0 temperature

dependence obtained for the CB9CB LC by Robles-Hernández et al. [32] (solid line) with the zero of the Haller function shifted at 363.2 K, which corresponds to the first temperature considered in the N_{tb} phase, below the biphasic region.

5. Conclusions

Upon cooling from the isotropic phase, EPR spectra of the CSL spin probe dissolved in the CB9CB liquid crystal confirmed the presence of a uniaxial nematic phase. Upon further cooling, the CB9CB liquid crystal exhibited a new phase that was no longer a monodomain. The EPR spectra clearly showed a non uniform local director organization that could be modelled as a collection of monodomains, tilted with respect to the magnetic field and orientationally distributed around the tilt direction. This result is compatible with the commonly accepted description of the twist-bend phase [20,24,25] in a bulk sample in which the heliconical axis is not uniform due, e.g., to a relatively weak magnetic field, not able to fully align the local domains, resulting in the observed non uniform organization of the local tilted directors. Between the two nematic phases, a biphasic region of about 4 K was found. EPR spectra in this region could be consistently analysed assuming a temperature independent value of the molecular order parameter, $\langle P_2 \rangle$, of the order parameter of the domain directors, $\langle P_2 \rangle_d$, and of the tilt angle, θ_0. At the lower end of the biphasic region, a discontinuity in the value of $\langle P_2 \rangle$ was observed. This result is in keeping with the first-order nature of the N_{tb}-N_u transition. The value of the $\langle P_2 \rangle$ recovered in the N_{tb} phase is in line with earlier research for this system [32,48,50] whereas in the N_u phase slightly lower values were recovered.

The dependence of the reorientational dynamics on the reduced temperature, in the N_u phase, is essentially identical to that exhibited by the related dimer CB11CB obtained in a previous work [26]. This result appears to be quite reasonable given the similarity of the two molecules and the fact that the temperature interval of the N_u phase of the CB11CB LC has a width very similar to that of the CB9CB LC and is shifted by only about 5 K to higher temperatures. In the N_{tb} phase the dynamics slows down significantly, indicating a larger microscopic rotational viscosity compared to the N_u phase, in agreement with our previous result [26]. Interestingly, this increase of the microscopic viscosity is quite small when compared to an increase of the macroscopic viscosity of several orders of magnitude observed in the N_{tb} phase of the homologues CB11CB [47], CB9CB [48] and CB7CB [49]. This observation suggests that, when the system goes from the N_u to the N_{tb} phase, the macroscopic molecular organization changes substantially but the molecular scale environment experiences only a small change.

Finally, the tilt angle is close to zero at the N_{tb}-N_u transition, in agreement with a previous result obtained for the CB9CB LC [32] and for the related dimer CB7CB [52,53]. Across the N_{tb} phase, the tilt exhibits an almost linear temperature dependence which is clearly different from the Haller-type one determined previously [32]. In particular, the tilt reaches values in the range 25–30° which is in line with results obtained for the dimer CB7CB [52,53] and for the dimer DTC5C7 [25]. Values of the tilt angle in the range around 30° were also obtained in a previous work on the dimer CB11CB [26], but with a different dependence on the reduced temperature.

Acknowledgements

Disclosure statement

No potential conflict of interest was reported by the authors.

Funding

References

[1] Mandle RJ. The Shape of Things To Come: The Formation of Modulated Nematic Mesophases at Various Length Scales. Chem-Eur J. 2017;23:8771–8779.

[2] Paterson DA, Abberley JP, Harrison WT, et al. Cyanobiphenyl-based liquid crystal dimers and the twist-bend nematic phase. Liq Cryst. 2017;44:127–146.

[3] Dawood AA, Grossel MC, Luckhurst GR, et al. Twist-bend nematics, liquid crystal dimers, structure-property relations. Liq Cryst. 2017;44:106–126.

[4] Mandle RJ, Goodby JW. Does Topology Dictate the Incidence of the Twist-Bend Phase? Insights Gained from Novel Unsymmetrical Bimesogens. Chem-Eur J. 2016;22:18456–18464.

[5] Mandle RJ, Archbold CT, Sarju JP, et al. The Dependency of Nematic and Twist-bend Mesophase Formation on Bend Angle. Sci Rep. 2016;6:36682 1–12.

[6] Mandle RJ. The dependency of twist-bend nematic liquid crystals on molecular structure: a progression from dimers to trimers, oligomers and polymers. Soft Matter. 2016;12:7883–7901.

[7] Pocock EE, Mandle RJ, Goodby JW. Molecular shape as a means to control the incidence of the nanostructured twist bend phase. Soft Matter. 2018;14:2508–2514.

[8] Chen D, Nakata M, Shao R, et al. Twist-bend heliconical chiral nematic liquid crystal phase of an achiral rigid bent-core mesogen. Phys Rev E. 2014;89:022506 1–5.

[9] Sreenilayam SP, Panov VP, Vij JK, et al. The N_{tb} phase in an achiral asymmetrical bent-core liquid crystal terminated with symmetric alkyl chains. Liq Cryst. 2017;44:244–253.

[10] Lu Z, Henderson PA, Paterson BJA, et al. Liquid crystal dimers and the twist-bend nematic phase. The preparation and characterisation of the alpha,omega-bis(4-cyanobiphenyl-4 ′-yl) alkanedioates. Liq Cryst. 2014;41:471–483.

[11] Mandle RJ, Davis EJ, Lobato SA, et al. Synthesis and characterisation of an unsymmetrical, ether-linked, fluorinated bimesogen exhibiting a new polymorphism containing the N_{tb} or 'twist-bend' phase. Phys Chem Chem Phys. 2014;16:6907–6915.

[12] Mandle RJ, Davis EJ, Voll CCA, et al. The relationship between molecular structure and the incidence of the N_{tb} phase. Liq Cryst. 2015;42:688–703.

[13] Mandle RJ, Davis EJ, Archbold CT, et al. Apolar Bimesogens and the Incidence of the Twist-Bend Nematic Phase. Chem-Eur J. 2015;21:8158–8167.

[14] Greco C, Luckhurst GR, Ferrarini A. Molecular geometry, twist-bend nematic phase and unconventional elasticity: a generalised Maier-Saupe theory. Soft Matter. 2014;10:9318–9323.

[15] Vanakaras AG, Photinos DJ. A molecular theory of nematic-nematic phase transitions in mesogenic dimers. Soft Matter. 2016;12:2208–2220.

[16] Ferrarini A. The twist-bend nematic phase: molecular insights from a generalised Maier-Saupe theory. Liq Cryst. 2017;44:45–57.

[17] Paterson DA, Gao M, Kim YK, et al. Understanding the twist-bend nematic phase: the characterisation of 1-(4-cyanobiphenyl-4′-yloxy)-6-(4-cyanobiphenyl-4′-yl)hexane (CB6OCB) and comparison with CB7CB. Soft Matter. 2016;12:6827–6840.

[18] Archbold CT, Mandle RJ, Andrews JL, et al. Conformational landscapes of bimesogenic compounds and their implications for the formation of modulated nematic phases. Liq Cryst. 2017;44:2079–2088.

[19] Tomczyk W, Pajak G, Longa L. Twist-bend nematic phases of bent-shaped biaxial molecules. Soft Matter. 2016;12:7445–7452.

[20] Zhu C, Tuchband MR, Young A, et al. Resonant Carbon K-Edge Soft X-Ray Scattering from Lattice-Free Heliconical Molecular Ordering: Soft Dilative Elasticity of the Twist-Bend Liquid Crystal Phase. Phys Rev Lett. 2016;116:147803 1–6.

[21] Chen D, Porada JH, Hooper JB, et al. Chiral heliconical ground state of nanoscale pitch in a nematic liquid crystal of achiral molecular dimers. Proc Natl Acad Sci U S A. 2013; 110:15931–15936.

[22] Borshch V, Kim YK, Xiang J, et al. Nematic twist-bend phase with nanoscale modulation of molecular orientation. Nat Commun. 2013;4:2635 1–8.

[23] Meyer C, Luckhurst GR, Dozov I. Flexoelectrically Driven Electroclinic Effect in the Twist-Bend Nematic Phase of Achiral Molecules with Bent Shapes. Phys Rev Lett. 2013; 111:067801 1–5.

[24] Cestari M, Diez-Berart S, Dunmur DA, et al. Phase behavior and properties of the liquid-crystal dimer $1'',7''$-bis(4-cyanobiphenyl-4′-yl) heptane: A twist-bend nematic liquid crystal. Phys Rev E. 2011;84:031704 1–20.

[25] Stevenson WD, Ahmed Z, Zeng XB, et al. Molecular organization in the twist-bend nematic phase by resonant X-ray scattering at the Se K-edge and by SAXS,WAXS and GIXRD. Phys Chem Chem Phys. 2017;19:13449–13454.

[26] Miglioli I, Bacchiocchi C, Arcioni A, et al. Director configuration in the twist-bend nematic phase of CB11CB. J Mater Chem C. 2016;4:9887–9896.

[27] Freed JH. Theory of slow tumbling ESR spectra for nitroxides. In: Berliner LJ, editor. Spin Labeling. Theory and Applications. Chapter 3. New York (NY): Academic Press; 1976. p. 53–132.

[28] Bacchiocchi C, Miglioli I, Arcioni A, et al. Order and Dynamics Inside H-PDLC Nanodroplets: An ESR Spin Probe Study. J Phys Chem B. 2009;113:5391–5402.

[29] Gopee H, Cammidge A, Oganesyan V. Probing Columnar Discotic Liquid Crystals by EPR Spectroscopy with a Rigid-Core Nitroxide Spin Probe. Angew Chem Int Ed. 2013; 52:8917–8920.

[30] Panov VP, Balachandran R, Nagaraj M, et al. Microsecond linear optical response in the unusual nematic phase of achiral bimesogens. Appl Phys Lett. 2011;99:261903 1–3.

[31] Tripathi CSP, Losada-Pérez P, Glorieux C, et al. Nematic-nematic phase transition in the liquid crystal dimer CBC9CB and its mixtures with 5CB: A high-resolution adiabatic scanning calorimetric study. Phys Rev E. 2011;84:041707 1–7.

[32] Robles-Hernández B, Sebastián N, Rosario de la Fuente M, et al. Twist, tilt, and orientational order at the nematic to twist-bend nematic phase transition of $1'',9''$-bis(4-cyanobiphenyl-4′-yl) nonane: A dielectric, ^{2}H NMR, and calorimetric study. Phys Rev E. 2015;92:062505 1–16.

[33] Vecchi I, Arcioni A, Bacchiocchi C, et al. Expected and unexpected behavior of the orientational order and dynamics induced by azobenzene solutes in a nematic. J Phys Chem B. 2007;111:3355–3362.

[34] Arcioni A, Bacchiocchi C, Vecchi I, et al. A comparison of the effects of dispersed hydrophobic or hydrophilic aerosil nanoparticles on the order and dynamics of the 5CB liquid crystal. Chem Phys Lett. 2004;396:433–441.

[35] Meirovitch E, Freed JH. Analysis of slow-motional electron spin resonance spectra in smectic phases in terms of molecular configuration, intermolecular interactions, and dy-

namics. J Phys Chem. 1984;88:4995–5004.

[36] Carr SG, Khoo SK, Luckhurst GR, et al. On the ordering matrix for the spin probe (3-spiro[2′-N-oxyl-3′,3′-dimethyloxazolidine])-5-alpha-cholestane, in the nematic mesophase of 4,4′-dimethoxyazoxybenzene. Mol Cryst Liq Cryst. 1976;35:7–13.

[37] Freed JH. ESR lineshapes and saturation in the slow motional region. The stochastic Liouville approach. In: Muus LT, Atkins PW, editors. Electron Spin Relaxation in Liquids. Chapter 14. New York (NY): Plenum Press; 1972. p. 387–409.

[38] Schneider DJ, Freed JH. Calculating slow motional magnetic resonance spectra: a user's guide. In: Berliner LJ, Reuben J, editors. Spin Labeling. Theory and Applications. (Biological Magnetic Resonance; Vol. 8); Chapter 1. New York (NY): Plenum Press; 1989. p. 1–76.

[39] Berntsen J, Espelid TO, Genz A. Algorithm 698: DCUHRE: An Adaptive Multidemensional Integration Routine for a Vector of Integrals. ACM Trans Math Softw. 1991;17:452–456.

[40] Arcioni A, Tarroni R, Zannoni C. Global target analysis of fluorescence depolarization in model membranes using exponential splines. J Chem Soc-Faraday Trans. 1993;89:2815–2822.

[41] Bevington PR. Data Reduction and Error Analysis for the Physical Sciences. New York (NY): McGraw-Hill; 1969.

[42] Bacchiocchi C, Miglioli I, Arcioni A, et al. EPR Study of Order and Dynamics of the 5CB Liquid Crystal in an H-PDLC Device. Mol Cryst Liq Cryst. 2012;558:127–139.

[43] Bacchiocchi C, Foschi G, Miglioli I, et al. Nematic Director Configuration, Local Order and Microviscosity in a PSLC Cell. Mol Cryst Liq Cryst. 2015;614:2–10.

[44] Oganesyan V, Kuprusevicius E, Gopee H, et al. Electron Paramagnetic Resonance Spectra Simulation Directly from Molecular Dynamics Trajectories of a Liquid Crystal with a Doped Paramagnetic Spin Probe. Phys Rev Lett. 2009;102:013005 1–4.

[45] Beguin L, Emsley JW, Lelli M, et al. The Chirality of a Twist-Bend Nematic Phase Identified by NMR Spectroscopy. J Phys Chem B. 2012;116:7940–7951.

[46] Emsley JW, Lesot P, Luckhurst GR, et al. Chiral solutes can seed the formation of enantiomorphic domains in a twist-bend nematic liquid crystal. Phys Rev E. 2013;87:040501 1–4.

[47] Balachandran R, Panov VP, Vij JK, et al. Elastic properties of bimesogenic liquid crystals. Liq Cryst. 2013;40:681–688.

[48] Hoffmann A, Vanakaras AG, Kohlmeier A, et al. On the structure of the Nx phase of symmetric dimers: inferences from NMR. Soft Matter. 2015;11:850–855.

[49] Cifelli M, Domenici V, Dvinskikh SV, et al. The twist-bend nematic phase: translational self-diffusion and biaxiality studied by ^{1}H nuclear magnetic resonance diffusometry. Liq Cryst. 2017;44:204–218.

[50] Zhang Z, Panov VP, Nagaraj M, et al. Raman scattering studies of order parameters in liquid crystalline dimers exhibiting the nematic and twist-bend nematic phases. J Mater Chem C. 2015;3:10007–10016.

[51] Haller I. Thermodynamic and static properties of liquid crystals. Prog Solid State Chem. 1975;10:103–118.

[52] Meyer C, Luckhurst GR, Dozov I. The temperature dependence of the heliconical tilt angle in the twist-bend nematic phase of the odd dimer CB7CB. J Mater Chem C. 2015; 3:318–328.

[53] Singh G, Fu J, Agra-Kooijman DM, et al. X-ray and Raman scattering study of orientational order in nematic and heliconical nematic liquid crystals. Phys Rev E. 2016; 92:060701 1–6.
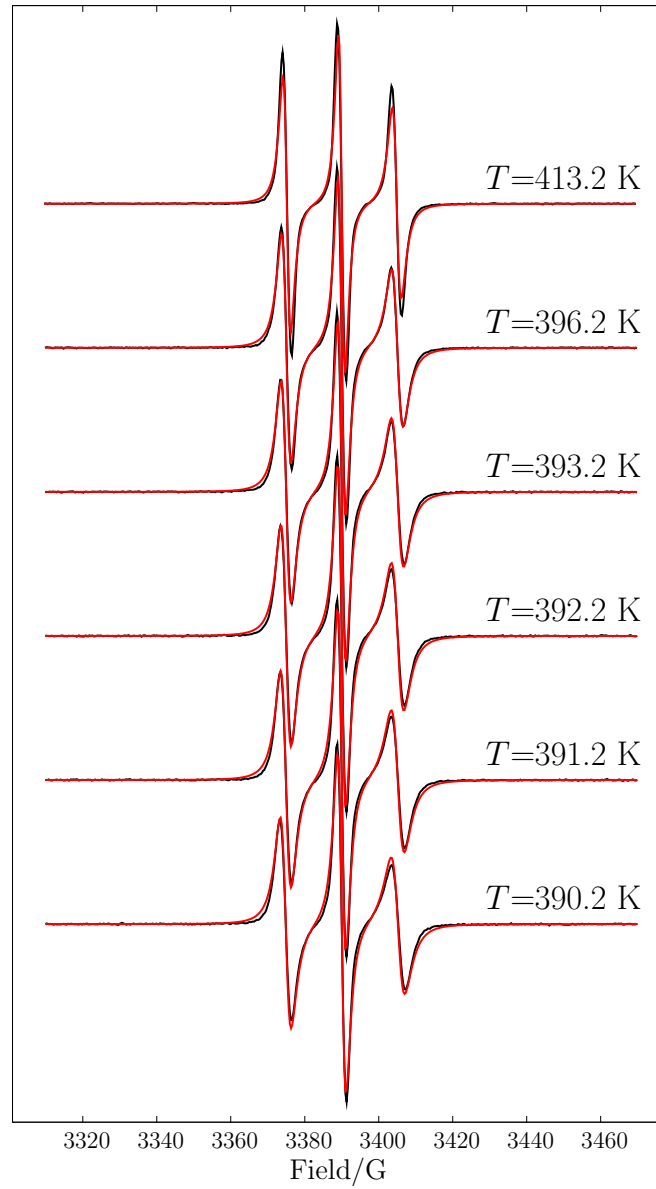
Figure 4. EPR spectra in the I phase of CB9CB (black line) and fit to the isotropic model (red line).
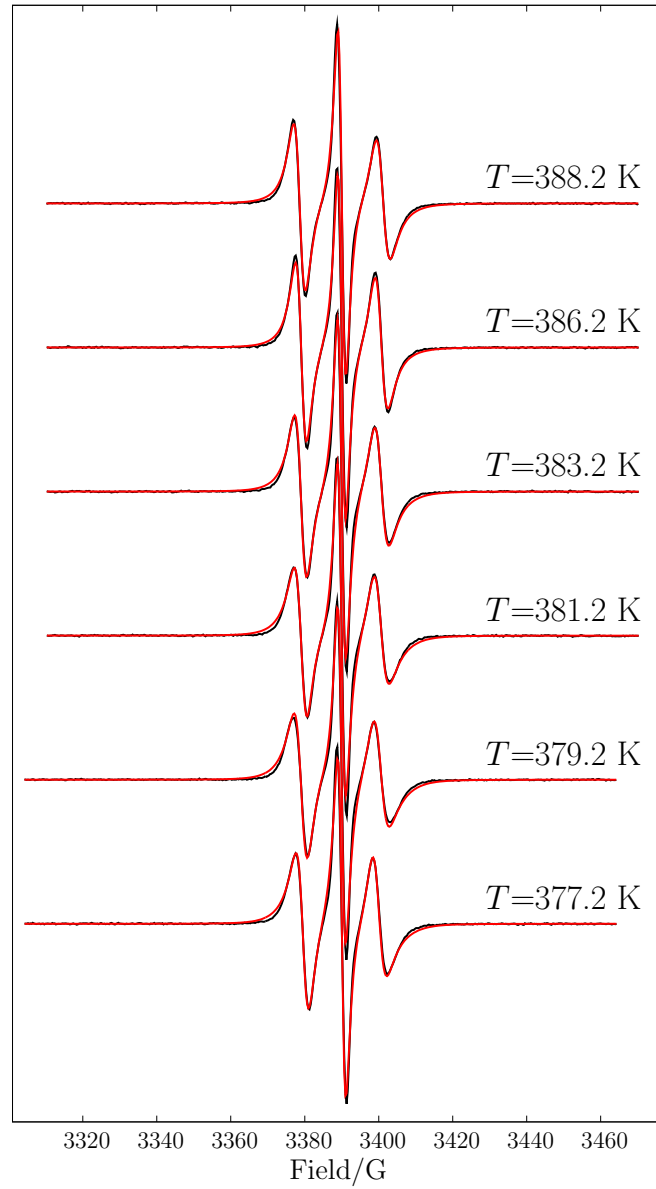
Figure 5. EPR spectra in the N$_u$ phase of CB9CB (black line) and fit to the uniaxial nematic monodomain model (red line).
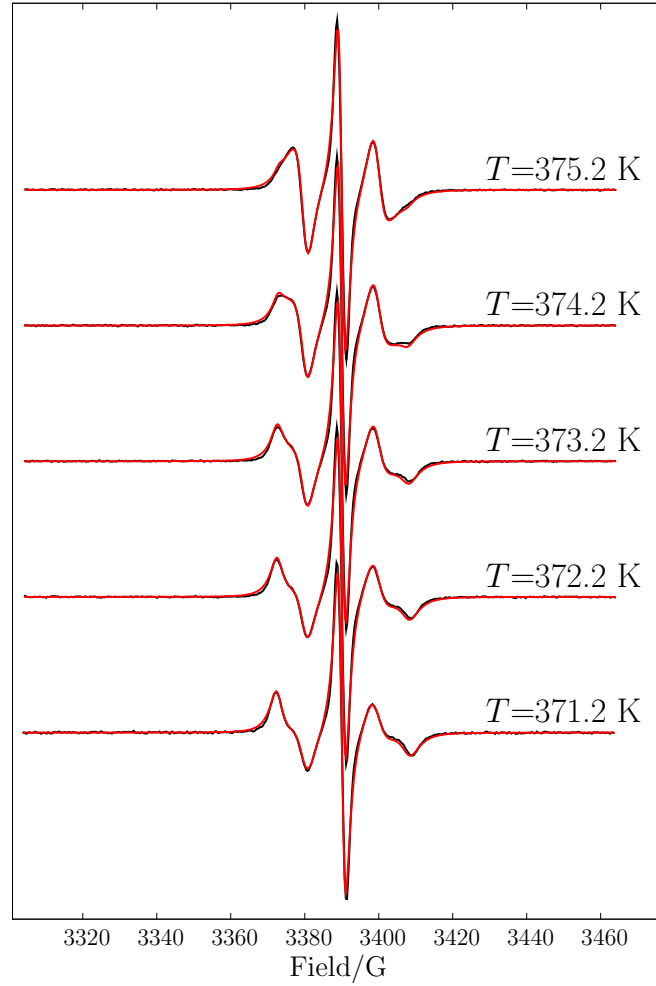
Figure 6. EPR spectra (black line) in the biphasic region of CB9CB, across the N_{tb}–N_u transition, and global fit (red line) to a model formed by two spectral contributions: one for the N_u phase, calculated according to the uniaxial nematic monodomain model, the other for the N_{tb} phase, calculated according to the distributed tilt (DT) model, presented earlier [26] (see text for details).
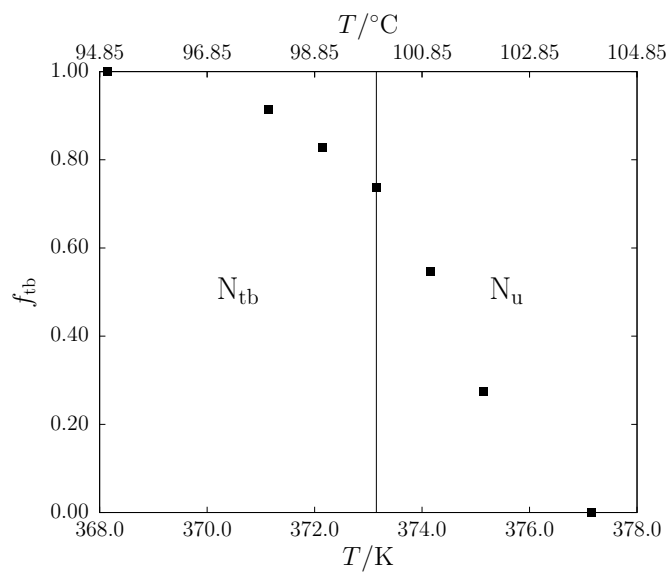
Figure 7. Temperature dependence of the fractional contribution of the spectral component due to the N_{tb} phase, f_{tb}, across the biphasic region of CB9CB, obtained from the global fit presented in Figure 6 (see text for details).
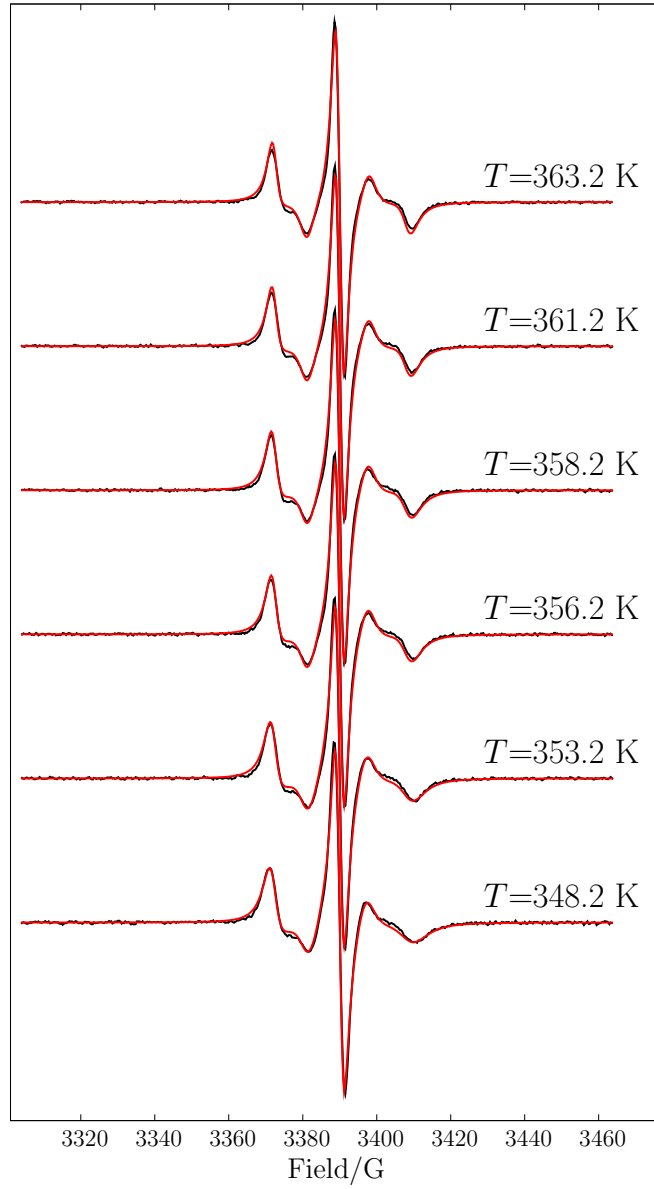
Figure 8. EPR spectra in the N_{tb} phase (black line) and fit to the distributed-tilt (DT) model (red line). Local $\langle P_2 \rangle$ was assumed to be independent of the temperature and treated as a global parameter. Best-fit value was 0.61. Best-fit values of the tilt angle, θ_0, are presented in Figure 11 (open squares, see text for details).
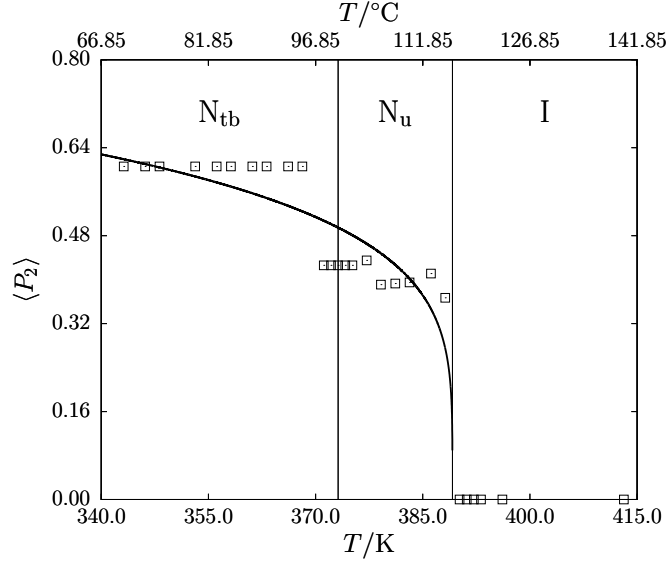
Figure 9. Temperature dependence of the local orientational order parameter, $\langle P_2 \rangle$, across the full temperature range studied (open squares), compared with values calculated with the Haller function of equation 7 ($T_{NI} = 389.2$ K, $\langle P_2 \rangle_0 = 0.97$, $\beta = 0.21$, solid line, see text for details). Vertical lines indicate the approximate transition temperatures observed, that are about 4 K below the transitions observed by Tripathi et al. [31] for pure CB9CB. In the biphasic region (series of five points centred on the N_{tb}–N_u transition), $\langle P_2 \rangle$ best-fit value was 0.43 for the N_u phase (data points shown) and 0.39 for the N_{tb} phase (not shown).
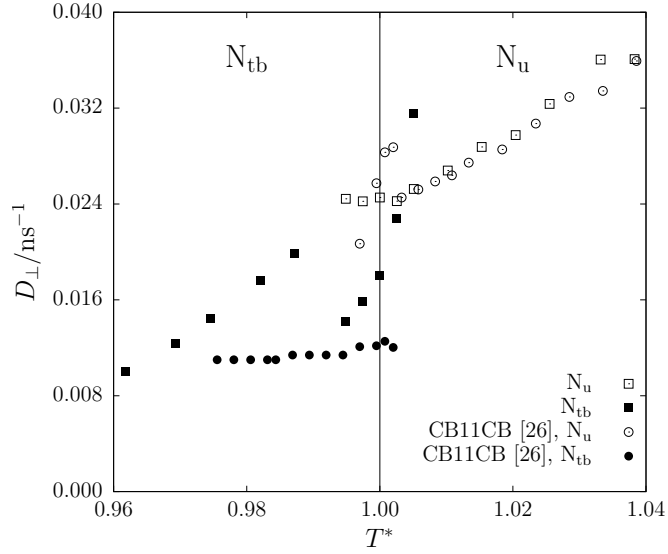
Figure 10. Dependence of the perpendicular component of the rotational diffusion tensor, $D_\perp$, on the reduced temperature, $T^* \equiv T/T_{N_{tb}-N_u}$, in the N_u phase (open squares) and in the N_{tb} phase (solid squares) compared to the values obtained for the related LC CB11CB [26] (open and solid circles). The vertical line indicates the approximate transition temperature observed, which is about 4 K below the transition observed by Tripathi et al. [31] for pure CB9CB. In the N_u phase, values for the CB9CB LC (open squares) are essentially identical to those for the CB11CB LC (open circles). Across the biphasic region, centred on the transition, the reorientational dynamics of the N_{tb} phase (solid symbols) is slower than that of the N_u phase (open symbols). In the N_{tb} phase, the reorientational dynamics of both LCs has values of the same order of magnitude and shows a further, almost linear decrease with the temperature (see text for details).
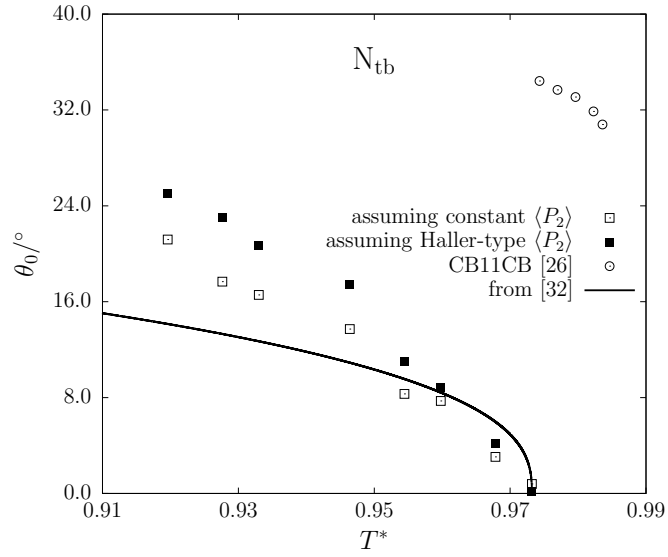
Figure 11. Dependence of the tilt angle, θ_0, on the reduced temperature, $T^* \equiv T/T_{\mathrm{N_{tb}-N_u}}$. The values were recovered from fits of the spectra recorded in the $\mathrm{N_{tb}}$ phase, below the biphasic region, by adopting two different globalization schemes (open and solid squares) and are compared to the values obtained for the related LC CB11CB [26] (open circles) and to the Haller-type θ_0 temperature dependence obtained for the CB9CB LC by Robles-Hernández et al. [32] (solid line) with the zero of the Haller function shifted at 363.2 K, which corresponds to the first temperature considered in the $\mathrm{N_{tb}}$ phase, below the biphasic region. In the first globalization scheme (open squares), the local $\langle P_2 \rangle$ was assumed to be constant across the $\mathrm{N_{tb}}$ phase, below the biphasic region. In the second (solid squares), the local $\langle P_2 \rangle$ had the empirical Haller-type temperature dependence of equation 7 ($T_{NI} = 389.2$ K, $\langle P_2 \rangle_0 = 0.97$, $\beta = 0.21$), shown as a solid line in Figure 9 (see text for details).